Analysis Model for Magnetic Energy Harvesters

Jinyeong Moon, Steven B. Leeb
Department of Electrical Engineering and Computer Science
Massachusetts Institute of Technology
Cambridge, MA 02139, USA

***Abstract*—Energy harvesting offers an important design option for creating sensing and control elements without a requirement for custom wiring or batteries. This paper presents an approach and design method for a magnetic energy harvester, VAMPIRE [1], whose magnetic core periodically goes into saturation. Saturating the core at appropriate times is essential for maximizing energy transfer. Methods for estimating the amount of harvested power under saturation using a "transfer window" are introduced. The accurate model for numerical simulation is also presented, and verified through experiments.**

***Index Terms*—Magnetic, Energy, Power, Harvest, Saturation, Nonlinear, Nonideal, Transformer, Inductor, Transfer, Window**

I. Introduction

Fine grain sensing and control is the future of energy efficiency. Electromechanical systems can waste energy for a variety of reasons. They may be operated poorly, e.g., left operating or operating at an inappopriate setpoint when not needed. Many electromechanical systems operate under closed-loop feedback control, which can be a disaster for efficient operation in pathological situations. HVAC components, for example, operate to achieve a comfort setpoint, and, without intervention, will continue to do so regardless of a developing but not-yet-crippling failure like loss of refrigerant charge. Distributed sensing can provide a detailed look at operations, and, with appropriate signal processing, can provide actionable information for preserving mission capability and operational efficiency.

Sensors and control elements require power and communication paths that can quickly create a dizzying requirement for new or additional wiring. Energy harvesting is an important solution to this problem, allowing adequately low-power sensors and controls to operate from power "sources" derived from parastic or symbiotic energy flows like mechanical vibration [5], [6], [10], thermal gradients [7], [8], acoustic vibrations [9], and light [11]. We are examining coupling magnetic fields from operating electromechanical equipment like rotating machines to create an inductive energy harvester. This harvester can power sensors for assessing vibration, thermal profile, and other operating signatures that can either indicate diagnostic conditions or affirm proper operation. When possible, inductive coupling can provide a relatively large amount of harvested energy compared to many other approaches, and has the additional benefit of allowing the associated sensor to measure the electrical consumption of the operating electromechanical load.

A core-clamp current transformer is a familiar solution for inductive coupling to a current-carrying wire. Magnetic cores are often used to make current sensors, and linearity, or at least the avoidance of severe nonlinearity like saturation, is generally important for current sensors. In contrast, for power harvesting, we have found that a saturating core can be essential for maximizing the energy harvested. In magnetic amplifiers [12], or saturable reactor applications, such as [13], [14], [15], and [16], magnetic cores are intentionally saturated during the operation, but they are used for changing the insertion impedance to act as switches, not harvesting power.

Saturation is highly nonlinear, and this paper presents a model of core behavior, including such nonlinearity, that can accurately predict the amount of power harvested from the environs of a current-carrying power wire, e.g., in the terminal connection box of a motor. Specifically, the model can be used as quick design aids or for more detailed numerical solution to meet an energy harvesting target.

II. VAMPIRE

We have developed a vibration and temperature monitoring system called VAMPIRE, vibration assessment monitoring point with integrated recovery of energy [1], [2]. VAMPIRE occupies free space in the terminal box of a typical motor enclosure, and can be added "new" or as a retrofit to an existing motor by passing a single phase wire through a VAMPIRE device. A magnetic core inductively couples energy from the phase wire, similar to a common current transformer but different in that here the goal is to actively extract desired power. While transformers are often operated to avoid saturation, controlled saturation is critical to extracting energy in the harvester application. High core permeability is essential to achieve acceptable winding coupling and adequate harvesting opportunity. Saturation occurs when voltage is intentionally developed on the secondary winding to transfer power. The timing of core saturation with respect to the AC primary side greatly affects the energy recovery. The core saturation complicates analytical modeling, giving rise to a need for a tractable model that can guide design.

Consider the following physical connection as in Fig. 1. The primary side is a single utility phase line at $60\,\mathrm{Hz}$ (or $50\,\mathrm{Hz}$), which supplies power to equipment to be monitored, e.g., a motor. The secondary side has N windings and is used to extract energy. The primary side current generates the magnetic field (H) and the flux density (B) inside the core, which induces voltage and current on the secondary side. Typically, the insertion impedance of the harvester is relatively low, and the primary wire can be thought as a current source created by

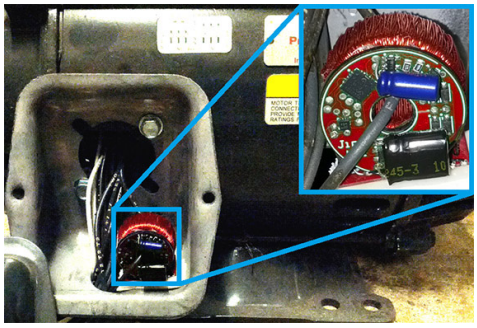

Fig. 1. VAMPIRE physical connection - real example

TABLE I
CORE DIMENSIONS

Outer Radius (r_{OD})	12.25 mm
Inner Radius (r_{ID})	8.25 mm
Height (h)	9 mm
Flux Area (A_{CORE})	3.6×10^{-5} m^2
Flux Length (l_{FLUX})	6.44×10^{-2} m

the operation of the electromechanical load. If the secondary side carries nonzero current, then it also generates H and affects B inside the core, creating a familiar coupled system. In steady-state operation, the combined winding system is governed by Maxwell's equations and the B-H characteristics of the core.

Experiments to validate our analysis procedure were conducted with a magnetic core. High permeability is essential for good coupling prior to saturation, and our illustrative design here uses an amorphous nanocrystalline core (VITROPERM-W380) by Vacuumschmelze (VAC) [3]. The dimensions of this core are listed in Table I.

III. Approximate Power Harvesting Analysis

In normal applications, magnetic cores are operated in a relatively unsaturated region of the B-H loop. If the core material enters the relatively saturated region in a transformer application, the voltage across the secondary rapidly drops to zero since the voltage that can be developed by the core is proportional to the time derivative of B. In this case, power delivery across the transformer essentially halts. In a current transformer application, if the primary side carries periodic current with sufficient amplitude to create adequate H field to drive the core into saturation, transformer current is transferred into the load only for a portion of the periodic cycle where the core is not saturated. The period of time when the core is able to transfer power might be termed a "transfer window".

In the next two subsections, we explore the harvestable power based on the extent of the transfer window. This approach enables quick hand calculations for core size and load target. More accurate numerical analyses for fine-tuning a design are presented in the following sections. For both the approximate and numerical approaches, we consider two possible load types: resistive loads, and constant voltage load (with an ideal rectifier, i.e., a regulated DC load).

A. Resistive Load (R_{LOAD}) Case

If the primary side current is a sinusoid with frequency of $\omega/2\pi$, the power delivered to the resistor pulsates at twice this frequency. The average power delivered to the load in each half cycle of the primary waveform can be computed given various assumptions about core saturation. The primary side period, the unsaturated time duration (transfer window) in each half cycle, and the time point beginning a half cycle are denoted as T, t_{SAT}, and t_0, respectively.

$$\begin{aligned} P_{\text{LOAD}} &= \frac{2}{T}\int_{t_0}^{t_0+t_{\text{SAT}}} \left[\frac{I_{\text{P}}}{N}\sin(\omega\, t)\right]^2 \cdot R_{\text{LOAD}}\ \mathrm{d}t \\ &= \frac{I_{\text{P}}^2 \cdot R_{\text{LOAD}}}{\pi\, N^2}\left[\frac{\omega\, t_{\text{SAT}}}{2} - \frac{\sin(2\,\omega\, t_{\text{SAT}})}{4}\right] \end{aligned} \tag{1}$$

When the core does not saturate ($t_{\text{SAT}} = T/2$), the average power harvest simply becomes

$$P_{\text{LOAD, nonsat}} = \frac{I_{\text{P}}^2 \cdot R_{\text{LOAD}}}{2\, N^2} \tag{2}$$

More generally, the core will saturate. To figure out t_{SAT}, we balance a flux equality between the maximally allowed flux set by B_{SAT} for the core and the applied voltage integrated over $T/2$. To align the zero crossings of the primary current and the power calculation, we set the initial time point (t_0) to be 0. Then, the voltage integration is from 0 to t_{SAT}.

$$\begin{aligned} 2\, B_{\text{SAT}}\, A_{\text{CORE}}\, N &= \int_0^{t_{\text{SAT}}} V_{\text{CORE}}(t)\ \mathrm{d}t \\ &= \int_0^{t_{\text{SAT}}} \frac{I_{\text{P}}}{N}\sin(\omega\, t)\cdot R_{\text{LOAD}}\ \mathrm{d}t \end{aligned} \tag{3}$$

The coefficient '2' before B_{SAT} on the left hand side comes from the fact that the core goes from one end of the B-H loop to the other end of the B-H loop in a half cycle, which results in a net change of $2\, B_{\text{SAT}}$. Solving (3) gives

$$t_{\text{SAT}} = \min\left[\frac{1}{\omega}\cos^{-1}\left(1 - \frac{2\,\omega\, B_{\text{SAT}}\, A_{\text{CORE}}\, N^2}{I_{\text{P}}\, R_{\text{LOAD}}}\right),\ \frac{T}{2}\right] \tag{4}$$

Since t_{SAT} is bounded by $T/2$, we can find the minimum R_{LOAD} that saturates the core, given I_{P} and N.

$$R_{\text{LOAD,min,sat}} = \frac{\omega\, B_{\text{SAT}}\, A_{\text{CORE}}\, N^2}{I_{\text{P}}} \tag{5}$$

In another special case where the core is heavily saturated, relatively early in the half cycle ($t_{\text{SAT}} \ll T/2$), we can approximate the sinusoidal current in (3) as a linear function around zero.

$$2\, B_{\text{SAT}}\, A_{\text{CORE}}\, N \approx \int_0^{t_{\text{SAT}}} \frac{I_{\text{P}}}{N}\,\omega\, t\cdot R_{\text{LOAD}}\ \mathrm{d}t \tag{6}$$

In this hard saturation regime, we can easily obtain an expersion for t_{SAT} without an inverse cosine function.

$$t_{\text{SAT, hardsat}} \approx \sqrt{\frac{4\, B_{\text{SAT}}\, A_{\text{CORE}}\, N^2}{\omega\, I_{\text{P}}\, R_{\text{LOAD}}}} \tag{7}$$

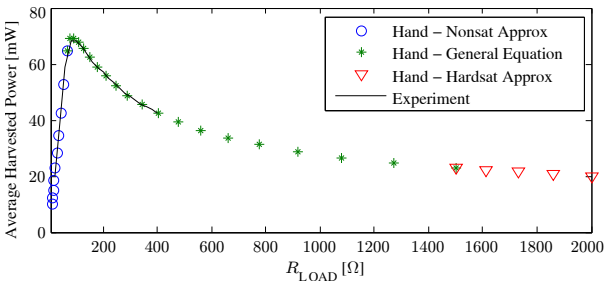

Fig. 2. P_{LOAD} response with a resistive load

Then, the average power harvest becomes

$$\begin{aligned} P_{\text{LOAD, hardsat}} &\approx \frac{2}{T}\int_0^{t_{\text{SAT}}} \left[\frac{I_{\text{P}}}{N}\,\omega\,t\right]^2 \cdot R_{\text{LOAD}}\ \mathrm{d}t \\ &= \frac{8}{3\,\pi}\,\frac{\omega^{1.5}\,I_{\text{P}}^{0.5}\,B_{\text{SAT}}^{1.5}\,A_{\text{CORE}}^{1.5}\,N}{R_{\text{LOAD}}^{0.5}} \end{aligned} \tag{8}$$

If we compare (2) to (8), we can see the two expressions have opposite dependencies on R_{LOAD}. The harvestable power increases with R_{LOAD} in the nonsaturation regime, and decreases with R_{LOAD} in the hard saturation regime. Therefore, we can expect that the peak will occur between two extremes.

However, finding the exact R_{LOAD} value for the maximum power harvest is challenging because the expression for P_{LOAD} is a complex function of t_{SAT}, and t_{SAT} also contains R_{LOAD} inside an inverse cosine function. If we find an extrema using (1) and (4), the following equation set is obtained, which can be solved numerically to find the R_{LOAD} that yields a maximum power harvest:

$$\begin{cases} R_{\text{LOAD}} &= \dfrac{2\,\omega\,t_{\text{SAT}} - \sin(2\,\omega\,t_{\text{SAT}})}{1-\cos(2\,\omega\,t_{\text{SAT}})} \\ &\quad \times \dfrac{\omega\,B_{\text{SAT}}\,A_{\text{CORE}}\,N^2\sin(\omega\,t_{\text{SAT}})}{I_{\text{P}}\,[1-\cos(\omega\,t_{\text{SAT}})]^2} \\ t_{\text{SAT}} &= \dfrac{1}{\omega}\cos^{-1}\left(1-\dfrac{2\,\omega\,B_{\text{SAT}}\,A_{\text{CORE}}\,N^2}{I_{\text{P}}\,R_{\text{LOAD}}}\right) \end{cases} \tag{9}$$

Fig. 2 illustrates an example with $I_{\text{P}} = 6.27\,\text{A}_{\text{RMS}}$, $N = 200$, and $\text{freq} = 60\,\text{Hz}$. We can see that (8) is a very close approximation to (1) when R_{LOAD} is relatively large, i.e., where the core enters hard saturation. We can also verify that the maximum power harvest indeed happens in the soft saturation regime, the region in between the two extremes. The solid black line indicates the experimental result.

B. Constant Voltage Load (V_{LOAD}) Case

For powering sensors and signal processing hardware, the energy harvester will likely provide power to a conversion or storage stage, not just a resistor. If a DC-DC converter with a switching frequency much higher than the line frequency is connected to the core as a load, the voltage across the core is effectively the cycle average of the input voltage of the converter, and it can be considered as a constant DC value to the core. Similarly, if a supercapacitor is used, due to its extremely high capacitance and the efforts of a post-regulator, the harvester again sees essentially constant DC voltage. In these cases, the important parameter for determining power transfer is the load voltage V_{LOAD}.

The calculation of the flux equality is much simpler now due to the time independent load voltage.

$$2\,B_{\text{SAT}}\,A_{\text{CORE}}\,N = \int_0^{t_{\text{SAT}}} V_{\text{LOAD}}\ \mathrm{d}t \tag{10}$$

Therefore,

$$t_{\text{SAT}} = \min\left[\frac{2\,B_{\text{SAT}}\,A_{\text{CORE}}\,N}{V_{\text{LOAD}}},\ \frac{T}{2}\right] \tag{11}$$

The average power harvest can be generally expressed as

$$\begin{aligned} P_{\text{LOAD}} &= \frac{2}{T}\int_0^{t_{\text{SAT}}} \left[\frac{I_{\text{P}}}{N}\sin(\omega\,t)\right]\cdot V_{\text{LOAD}}\ \mathrm{d}t \\ &= \frac{I_{\text{P}}\,V_{\text{LOAD}}}{\pi\,N}\,[1-\cos(\omega\,t_{\text{SAT}})] \end{aligned} \tag{12}$$

Using (12), we can calculate the average power harvest of the special case where the core does not saturate ($t_{\text{SAT}} = T/2$).

$$P_{\text{LOAD, nonsat}} = \frac{2\,I_{\text{P}}\,V_{\text{LOAD}}}{\pi\,N} \tag{13}$$

Also, we can express the average power harvest in hard saturation ($t_{\text{SAT}} \ll T/2$):

$$\begin{aligned} P_{\text{LOAD, hardsat}} &\approx \frac{2}{T}\int_0^{t_{\text{SAT}}} \left[\frac{I_{\text{P}}}{N}\,\omega\,t\right]\cdot V_{\text{LOAD}}\ \mathrm{d}t \\ &= \frac{2\,\omega^2\,I_{\text{P}}\,B_{\text{SAT}}^2\,A_{\text{CORE}}^2\,N}{\pi\,V_{\text{LOAD}}} \end{aligned} \tag{14}$$

Again, the expressions for the average power harvest in the two extremes have opposite dependencies on V_{LOAD}. The peak will occur in between unsaturated and hard saturated operation. The maximum power harvest point is relatively easily found in the voltage load case. We differentiate P_{LOAD} with V_{LOAD}, which gives the following equation to solve for extrema:

$$\begin{aligned} 0 =& 1-\cos\left(\frac{2\,\omega\,B_{\text{SAT}}\,A_{\text{CORE}}\,N}{V_{\text{LOAD}}}\right) \\ &- \frac{2\,\omega\,B_{\text{SAT}}\,A_{\text{CORE}}\,N}{V_{\text{LOAD}}}\sin\left(\frac{2\,\omega\,B_{\text{SAT}}\,A_{\text{CORE}}\,N}{V_{\text{LOAD}}}\right) \end{aligned} \tag{15}$$

Equation (15) is in the form:

$$1-\cos(x) - x\cdot\sin(x) = 0 \tag{16}$$

This type of equation has an obvious but nonpractical solution at $x = 0$. An additional condition on x can be inferred:

$$x = \frac{2\,\omega\,B_{\text{SAT}}\,A_{\text{CORE}}\,N}{V_{\text{LOAD}}} = \omega\,t_{\text{SAT}} \le \omega\,\frac{T}{2} = \pi \tag{17}$$

Based on (17), the trace of $1-\cos(x)-x\cdot\sin(x)$ is drawn on Fig. 3 up to $x = \pi$. As shown in the figure, it has a single nonzero solution at $x = 2.3311224$. Using $3\pi/4$ as an approximate solution, the optimum V_{LOAD} can be expressed as

$$V_{\text{LOAD,pmax}} \approx \frac{8}{3\pi}\cdot\omega\,B_{\text{SAT}}\,A_{\text{CORE}}\,N \tag{18}$$

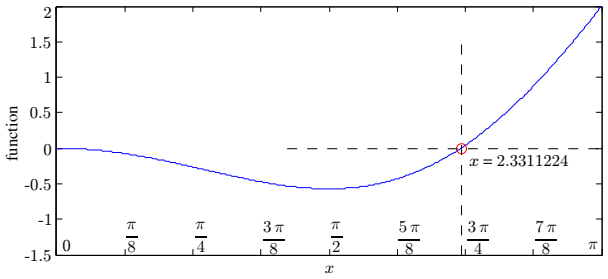

Fig. 3. Trace of $1 - \cos(x) - x \cdot \sin(x)$

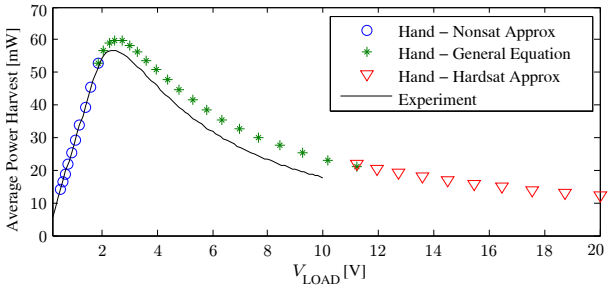

Fig. 4. P_{LOAD} response with a constant voltage load

And the corresponding maximum power harvest is

$$P_{\text{LOAD,max}} \approx \frac{8\,(2+\sqrt{2})}{6\,\pi^2} \cdot \omega\, I_{\text{P}}\, B_{\text{SAT}}\, A_{\text{CORE}} \tag{19}$$

Figure 4 illustrates an example with $I_{\text{P}} = 6.27\,\text{A}_{\text{RMS}}$, $N = 200$, and $\text{freq} = 60\,\text{Hz}$. As expected, the maximum power harvest happens in between the unsaturated operation region and the hard saturation region. The expression of $P_{\text{LOAD, max}}$ is independent of the magnetic permeability (μ) of the core. However, it is implied in the region itself that the core must be placed in saturation. Therefore, μ needs to be sufficiently high so that it can drive B from $-B_{\text{SAT}}$ to $+B_{\text{SAT}}$ within the given range of the input current. Essentially, high μ improves coupling to the primary current, and soft saturation is desirable for maximum power harvest.

The horizontal location of the peak is similar in both the estimates and the experimental results. The estimate is slightly "off" in predicting peak power and into the saturation region. This error, relative to the analysis for the resistive case, occurs because of the voltage load. In the case of the resistive load, the load voltage, which is directly seen by the core, is proportional to the transformer current until saturation. Therefore, the flux accumulation will be negligble when the transformer current is near zero. An error in determining the start of the cycle, if any, will have little effect, and the end point of the transfer window will be essentially correctly estimated. On the other hand, for the voltage load case, as soon as the secondary current flows, the fixed load voltage is applied across the core, and develops core flux at the same rate regardless of the level of the transformer current. Therefore, any mis-estimate in the start time of the transfer window, e.g., which opens up the transfer window a little earlier by Δt compared to the idealized analysis, will shift the end point of the transfer window by the same amount, Δt, to an earlier time point. In the worst case, where the transfer window ends at the peak of the sinusoid, the loss is substantial: the maximum current that can possibly flow in a time segment as long as Δt is lost due to the transfer window shift, and, instead, we "gain" a longer interval with near-zero current in the start of the transfer window. This issue tends to be worse in the hard saturation regime because the transfer window is shorter.

In practice, the transfer window "opens" early because of the core coming out of the saturation ahead of the primary current zero crossing. Once the core gets out of the tail region of the B-H loop, which is slightly before the zero crossing of the transformer current in the experiment, high magnetizing inductance is restored, and slows the change of the magnetizing current. Since the magnetizing current cannot rapidly track the transformer current, the current difference between them must be flown into the load resistor. As soon as a current difference is generated, the core directly sees the load voltage, and starts "accumulating" flux.

The following sections introduce a model to accurately predict the amount of power harvest. Nonidealities caused by a nonlinear core behavior are included in the model, and computed through numerical methods.

IV. Nonlinear Modeling

We present a core model that can be used in a numerical solver to predict behavior of the harvester with excellent accuracy. The model, derived from Maxwell's equations, is especially useful for refining a target design. Nonidealities such as hysteresis core loss and wire losses are considered.

A. Maxwell Model

Denoting the secondary side current as $I_{\text{S}}(t)$, the net ampere-turn seen by the core is

$$\text{AT}_{\text{CORE}} = I_{\text{P}} \sin(\omega\, t) - N \times I_{\text{S}}(t) \tag{20}$$

The primary side current is assumed sinusoidal AC with an amplitude of I_{P}. The magnetic field $H(r,t)$ in the core is

$$H(r,t) = \frac{\text{AT}_{\text{CORE}}(t)}{2\,\pi\, r} = \frac{I_{\text{P}} \sin(\omega\, t) - N\, I_{\text{S}}(t)}{2\,\pi\, r} \tag{21}$$

The magnetic flux density, B, is determined by the B-H curve of the core. We begin with a consideration of a saturating but non-hysteretic core, and expand to add hysteresis later. To model saturation, we can just use a piecewise linear waveform as in the left of Fig. 5, or, more practically, an 'arctan' function as in the right of Fig. 5. With the 'arctan' function, the magnetic flux density can be modeled as

$$\begin{aligned} B(r,t) &= B_{\text{SAT}} \cdot \frac{2}{\pi} \text{arctan}\left(\frac{H(r,t)}{\alpha}\right) \\ &= B_{\text{SAT}} \cdot \frac{2}{\pi} \text{arctan}\left(\frac{I_{\text{P}} \sin(\omega\, t) - N\, I_{\text{S}}(t)}{2\,\pi\, r\, \alpha}\right) \end{aligned} \tag{22}$$

Please note that $2/\pi$ is used to normalize the return value of arctan function to 1 when saturated. The reciprocal of α describes the sensitivity in the nonsaturated region. Its role is similar to the initial permeability in conventional models.

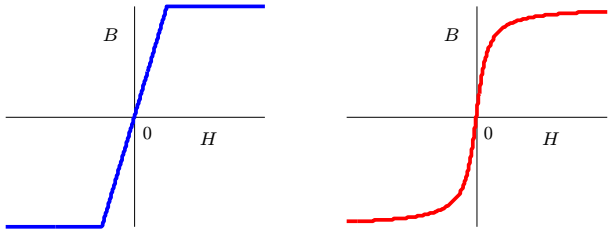

Fig. 5. B-H curves with saturation (left: piecewise linear / right: arctan)

If we denote the height, outer radius, and inner radius of the toroidal core as h, r_{OD}, and r_{ID}, respectively, we can express the voltage across the core as below.

$$V_{\text{CORE}}(t) = \int_{r_{\text{ID}}}^{r_{\text{OD}}} N \cdot h \cdot \frac{\partial B(r,t)}{\partial t}\, \mathrm{d}r \tag{23}$$

The time derivative of the magnetic flux density can be calculated by differentiating (22).

$$\frac{\partial B(r,t)}{\partial t} = \frac{B_{\text{SAT}}}{\pi^2\, r\, \alpha} \cdot \frac{\omega\, I_{\text{P}} \cos(\omega\, t) - N\, \dfrac{\partial I_{\text{S}}(t)}{\partial t}}{1 + \dfrac{[I_{\text{P}} \sin(\omega\, t) - N\, I_{\text{S}}(t)]^2}{4\,\pi^2\, r^2\, \alpha^2}} \tag{24}$$

When we integrate (24) over r from r_{ID} to r_{OD} , we can evaluate (23):

$$\begin{aligned} V_{\text{CORE}}(t) = & \frac{N \cdot h \cdot B_{\text{SAT}}}{2\pi^2 \alpha} \times \left[\omega\, I_{\text{P}} \cos(\omega t) - N \frac{\partial I_{\text{S}}(t)}{\partial t}\right] \\ & \times \ln\left(\frac{r_{\text{OD}}^2 + \dfrac{[I_{\text{P}} \sin(\omega t) - N\, I_{\text{S}}(t)]^2}{4\,\pi^2 \alpha^2}}{r_{\text{ID}}^2 + \dfrac{[I_{\text{P}} \sin(\omega t) - N\, I_{\text{S}}(t)]^2}{4\,\pi^2 \alpha^2}}\right) \end{aligned} \tag{25}$$

A hybrid circuit representation of (25) is given as a two-port box in a dashed line in Fig. 6. The leakage inductance is relatively small for the experimental core and is ignored in this figure. We model wire loss with R_{WIRE}, which is in series with the load. The effect of hysteresis on the harverster is included with a resistance R_{CORE} in parallel with the core. The detailed analyses for the values of these loss components are described shortly.

If we define the load charateristics in terms of $V_{\text{CORE}}(t)$ and $I_{\text{S}}(t)$, we have a complete set of differential equations that describes the system. Assuming the core is connected to an external circuit, a set of general system equations can be obtained by combining (25) and the following equations set:

$$\begin{cases} I_{\text{S}}(t) &= I_{\text{LOAD}}(t) + I_{\text{LOSS}}(t) \\ V_{\text{CORE}}(t) &= I_{\text{LOSS}}(t) \cdot R_{\text{CORE}} \\ V_{\text{CORE}}(t) &= I_{\text{LOAD}}(t) \cdot R_{\text{WIRE}} + V_{\text{LOAD}}(t) \end{cases} \tag{26}$$

We will illustrate the use of this model with a resistive load, with $V_{\text{LOAD}}(t) = I_{\text{LOAD}}(t) \cdot R_{\text{LOAD}}$, with the understanding that the load model can be extended to any load type, including switched loads, given an accurate load model, e.g., an equation relating $V_{\text{LOAD}}(t)$ and $I_{\text{LOAD}}(t)$. In the next section, we will discuss how to model the lossy elements, R_{WIRE} and R_{CORE}.

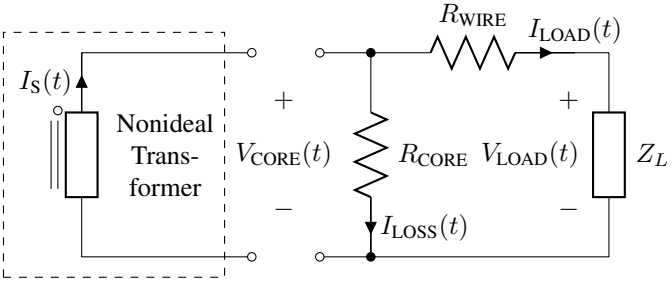

Fig. 6. Circuit representation of Maxwell method

B. Loss Modeling

1) Wire Loss Modeling: Primary currents for the harvester are typically (but not necessarily) from the power line of monitored equipment operating at line frequency. At 60 Hz, the skin depth of the copper wire is,

$$\delta = \sqrt{\frac{2\,\rho}{\omega\mu}} = \sqrt{\frac{2 \cdot 1.68 \times 10^{-8}}{2\,\pi\, 60 \cdot 4\,\pi \times 10^{-7}}} = 8.42\,\text{mm} \tag{27}$$

The wire diameter for the secondary windings is usually much smaller than 8.42 mm. For example, in our prototype design, we used AWG 30 with a diameter of 0.255 mm [1]. Because δ is much larger than the wire diameter, we can ignore skin effect, although this could be important in other applications. Following the analysis discussed in [4], the proximity effect is also negligible at the line frequency using this wire guage. As an example, assume AWG 30 with 500 turns and 3 layers. Each turn is roughly 42.5 mm long, and $R_{\text{DC}} = 7\,\Omega$. To convert the round-wire windings into equivalent foil conductors, we model each conductor with $N/3$ windings, and effective height of $2\,\pi\, r_{\text{ID}}$. The effective width of each "foil" is,

$$w_{eff} = \frac{\pi\, r_{\text{AWG30}}^2 \times N/3}{2\,\pi\, r_{\text{ID}}} = 0.164\,\text{mm} \tag{28}$$

And,

$$\Delta = \frac{w_{eff}}{\delta} = 0.0195 \tag{29}$$

With $M = 3$,

$$\begin{aligned} F_R = \frac{R_{\text{AC}}}{R_{\text{DC}}} = \Delta \cdot \Bigg[& \frac{\sinh(2\,\Delta) + \sin(2\,\Delta)}{\cosh(2\,\Delta) - \cos(2\,\Delta)} \\ & + \frac{2\,(M^2 - 1)}{3} \cdot \frac{\sinh(\Delta) - \sin(\Delta)}{\cosh(\Delta) + \cos(\Delta)} \Bigg] \end{aligned} \tag{30}$$

$$= \quad 1.00000$$

Therefore, the proximity effect is negligible, and we need only to include DC resistance for wire loss modeling.

2) Core Loss Modeling: As will be shown later, hysteresis loss for the VAC core will be so low that we can ignore it if the output power is larger than several mW. We discuss core loss here to provide a general model for cores with higher losses. Among many techniques to estimate core loss at given frequency and B_{PEAK} level [17], [18], [19], [20], [21], our core loss model is based on a simple expression of [17] due to zero DC-bias and symmetric B-H loop operations centered

at zero. The loss in our analysis is proportional to $f^1\,\hat{B}^2$ in principle, though the actual implementation is based on the cyclic measurements of B_{PEAK} and I_{PEAK}.

To model core loss, we make a rectangular approximation to the B-H curve. We track the peak load current (I_{PEAK}), the peak core voltage (hence B_{PEAK}), and the RMS voltage of the core (V_{RMS}) throughout each cycle. These values can be used to estimate a B-H loop area. In a numerical simulation, this power loss can be calculated and used to update the resulting core loss resistance for the next cycle. Assuming the core maintains its high permeability until saturation, where Volume is the volume of the core and H_C is the coercivity of the core, the full hysteresis loss is modeled as

$$P_{\text{LOSS-MAX}} = 2\,H_C \cdot 2\,B_{\text{SAT}} \cdot \text{Volume} \cdot \text{freq} \tag{31}$$

The B-H loop loss for any particular operating cycle can be calculated as a fraction of the maximum loss:

$$P_{\text{LOSS}} = P_{\text{LOSS-MAX}} \cdot \frac{I_{\text{PEAK}}}{I_{\text{SAT}}} \cdot \frac{B_{\text{PEAK}}}{B_{\text{SAT}}} \tag{32}$$

Finally, the loss resistance is

$$R_{\text{CORE}} = \frac{V_{\text{RMS}}^2}{P_{\text{LOSS}}} \tag{33}$$

This model calculation must be performed over a full cycle in order to permit calculation of the RMS values. We want the modeled resistor to dissipate the required amount of power over a cycle (or, if using a rectifier, a half cycle). However, adding such a resistor (or changing the loss resistance) will change the current divider formed with the magnetizing inductance, the core loss resistor, and the load. Since the entire circuit is continuously affected by cyclic update of the loss resistance, an additional numerical solver is used as an "internal loop" to provide a convergence to a correct core loss resistance, operating to provide correct values to the time-domain circuit solver.

C. Parameter Estimation

To demonstrate our model and approach for a numerical simulation, three parameters are required: B_{SAT}, α, and $P_{\text{LOSS-MAX}}$.

1) B_{SAT} Estimation: To characterize the core, we conduct experiment as depicted in Fig. 7, with a resistive load connected to the core. We need to select the load resistance high enough that the core goes into the hard saturation. If it is in hard saturation, the analysis simplifies in the sense that hysteresis loss is at maximum, which ensures that the core is driven to $\pm B_{\text{SAT}}$, and that a distinct "cat-ear" shape in voltage makes the waveforms easy to identify.

In a half cycle, $\Delta B = 2\,B_{\text{SAT}}$, hence $\Delta\Lambda = 2\,B_{\text{SAT}}\,A_{\text{CORE}}\,N$. This must be equal to the core voltage integrated over a half cycle. With a measurement of the load voltage over a half cycle, we can usefully write:

$$\frac{R_{\text{WIRE}} + R_{\text{LOAD}}}{R_{\text{LOAD}}} \cdot V_{\text{LOAD, AVG}} \cdot \frac{T}{2} = 2\,B_{\text{SAT}}\,A_{\text{CORE}}\,N \tag{34}$$

Therefore,

$$B_{\text{SAT}} = \frac{T\,(R_{\text{WIRE}} + R_{\text{LOAD}})}{4\,A_{\text{CORE}}\,N\,R_{\text{LOAD}}} \cdot V_{\text{LOAD, AVG}} \tag{35}$$

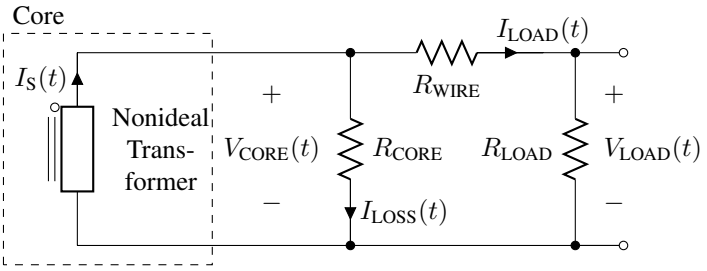

Fig. 7. Test circuit for the parameter estimation

2) $P_{LOSS\text{-}MAX}$ and α Estimation: We use the same circuit used for estimating B_{SAT} to determine core loss, and operate the core in saturation regime to ensure that the hystersis loss is at $P_{\text{LOSS-MAX}}$.

With a resistive load, we can simplify the general system equation set, (25) along with (26), to a single equation about $I_{\text{LOAD}}(t)$ as below.

$$\begin{aligned} &\frac{N\,h\,B_{\text{SAT}}}{2\,\pi^2\,\alpha} \times \left[\omega\,I_{\text{P}}\cos(\omega\,t) - \gamma\,N\frac{\partial I_{\text{LOAD}}(t)}{\partial t}\right] \\ &\times \ln\left(\frac{r_{\text{OD}}^2 + \dfrac{\left[I_{\text{P}}\sin(\omega t) - \gamma\,N\,I_{\text{LOAD}}(t)\right]^2}{4\,\pi^2\alpha^2}}{r_{\text{ID}}^2 + \dfrac{\left[I_{\text{P}}\sin(\omega t) - \gamma\,N\,I_{\text{LOAD}}(t)\right]^2}{4\,\pi^2\alpha^2}}\right) \\ =\;& I_{\text{LOAD}}(t)\cdot(R_{\text{WIRE}} + R_{\text{LOAD}}) \end{aligned} \tag{36}$$

where γ is defined as

$$\gamma = \frac{R_{\text{CORE}} + R_{\text{WIRE}} + R_{\text{LOAD}}}{R_{\text{CORE}}} \tag{37}$$

By evaluating (36) at two different time points, we generate two equations about α and γ. For the evaluations, we extract a full cycle data of the primary side current and $V_{\text{LOAD}}(t)$. The cosine and sine terms can be directly calculated with the selected time points, and $I_{\text{LOAD}}(t)$ can be calculated by $V_{\text{LOAD}}(t)/R_{\text{LOAD}}$. Note that zero crossings of the primary side current and $V_{\text{LOAD}}(t)$ do not align in general. When evaluating $V_{\text{LOAD}}(t)$ at two time points, the phase shift of $V_{\text{LOAD}}(t)$ with respect to the zero crossing of the primary side should be considered. We directly obtain α from solving two resulting equations. And, γ (with $V_{\text{LOAD,RMS}}$ that can be computed with the extracted cycle data) leads to:

$$P_{\text{LOAD-MAX}} = \frac{(\gamma - 1)\;V_{\text{LOAD,RMS}}^2}{R_{\text{WIRE}} + R_{\text{LOAD}}} \tag{38}$$

D. Magnetic Permeability (μ_r) Estimation

If we differentiate both sides of (22) with $H(r,t)$,

$$\frac{\partial B}{\partial H} = B_{\text{SAT}} \cdot \frac{2}{\pi} \cdot \frac{1}{\alpha} \cdot \frac{1}{1 + \dfrac{H^2}{\alpha^2}} \tag{39}$$

This equation is maximized when $H(r,t) = 0$, and this is the initial magnetic permeability, $\mu_0\,\mu_r$, at zero. Therefore,

$$\mu_r = \frac{2\,B_{\text{SAT}}}{\pi\,\alpha\,\mu_0} \tag{40}$$

Note of course that the nonlinear magnetizing inductance arises from the fact that that μ_r is an estimate of the initial permeability, and will not be maintained constant throughout the period.

V. Numerical Simulation

The numerical circuit simulator is implemented in MATLAB. The multi-dimensional Jacobian-free numerical solvers employed in the simulator are based on the Newton and the Generalized Conjugate Residual (GCR) [22], [23] methods, and find solutions of equations generated from the Maxwell core model, the core loss model, and the load model. The Newton method is used to find a zero crossing, i.e., solution, of a function, and the GCR is used to rapidly construct the search direction for the next Newton. At each iteration of the GCR, a vector orthogonal to those obtained from earlier iterations is added to the search direction. The progression in time, i.e., estimating the next time point for transient simulation, is modeled by trapezoidal integration.

We illustrate the resistive load case as an example. We rearrange (36) to get the first time derivative of $I_{\text{LOAD}}(t)$:

$$\frac{\partial I_{\text{LOAD}}(t)}{\partial t} = \frac{\omega\, I_{\text{P}}}{\gamma\, N}\cos(\omega t) - \frac{2\pi^2\alpha}{\gamma\, N^2\, h\, B_{\text{SAT}}}\times \frac{(R_{\text{WIRE}} + R_{\text{LOAD}})\cdot I_{\text{LOAD}}(t)}{\ln\left(\dfrac{r_{\text{OD}}^2 + \dfrac{\left[I_{\text{P}}\sin(\omega t) - \gamma\, N\, I_{\text{LOAD}}(t)\right]^2}{4\,\pi^2\alpha^2}}{r_{\text{ID}}^2 + \dfrac{\left[I_{\text{P}}\sin(\omega t) - \gamma\, N\, I_{\text{LOAD}}(t)\right]^2}{4\,\pi^2\alpha^2}}\right)} \tag{41}$$

Trapezoidal integration applied to $I_{\text{LOAD}}(t)$ is:

$$I_{\text{LOAD}}(t_{n+1}) - I_{\text{LOAD}}(t_n) = \frac{1}{2}\,\Delta t\left(\left.\frac{\partial I_{\text{LOAD}}(t)}{\partial t}\right|_{t=t_n} + \left.\frac{\partial I_{\text{LOAD}}(t)}{\partial t}\right|_{t=t_{n+1}}\right) \tag{42}$$

We combine (41) and (42), move all the terms to the same side, and define the resulting side as G. We can numerically solve $G = 0$ using Newton with GCR for each time point. The first order differential equation requires one initial condition. Since the primary side is a sine wave, its value is zero at $t = 0$, and if the system is fully de-energized, $I_{\text{LOAD}}(t)$ is zero as well. This initial condition produces a turn-on transient. After we obtain $I_{\text{LOAD}}(t)$ for the entire cycle, we calculate I_{PEAK}, B_{PEAK}, and $V_{\text{CORE, RMS}}$. Using the same steps discussed in (32) and (33), P_{LOSS} and R_{CORE} can be obtained.

However, two problems remain: first, we are interested in power harvesting capability in the steady-state, not the initial transient; second, the convergence regarding R_{CORE} and $V_{\text{CORE, RMS}}$ is not discussed. In order to guarantee the steady-state and the convergence on core loss, we add another solver with a shooting function F_{SHOOTING} that returns a 2×1 vector. The added solver also employs Newton with GCR, and wraps around the time range solver. The first element of the shooting function calculates the difference of two function values that are apart exactly by a period in time, and returns zero if it is in the steady-state.

$$F_{\text{SHOOTING}}[1] = I_{\text{LOAD}}(t_0 + T) - I_{\text{LOAD}}(t_0) \tag{43}$$

```
Until(|F_SHOOTING| ≤ Tolerance for F) {
   for each time point τ {
      Until(|G| ≤ Tolerance for G) {
         Newton_GCR on G;(residual update)
      }
      I_LOAD(τ) = Solved Value;
   }
   V_CORE,RMS Calculation;
   P_LOSS Calculation;
   Newton_GCR on F;(residual update)
}
```

Fig. 8. Pseudo code of the numerical simulator

TABLE II
Core Parameters

B_{SAT}	1.190 T
$P_{\text{LOSS-MAX}}$	0.125 mW
α	2.2

The second element calculates the difference between two core loss resistance values in two consecutive iterations. If the difference converges to zero, R_{CORE}, P_{LOSS}, and $V_{\text{CORE, RMS}}$ are in a correct relationship. $R_{\text{CORE-PREV}}$ denotes the core loss resistance calculated in the previous iteration.

$$F_{\text{SHOOTING}}[2] = \frac{V_{\text{CORE,RMS}}^2}{P_{\text{LOSS}}} - R_{\text{CORE-PREV}} \tag{44}$$

If $|F_{\text{SHOOTING}}|$ is within the tolerance, the system is in the steady-state, and the core loss is correctly estimated. Figure 8 describes the pseudo code including two solvers in separate layers and the shooting function.

VI. Experiments

An amorphous nanocrystalline core was used to verify the validity of the proposed modeling and analysis. The estimated parameter values, B_{SAT}, $P_{\text{LOSS-MAX}}$, and α, are listed in Table II. The manufacturer of the core is Vacuumschmelze.

In Fig. 9, four plots are presented to portray the close agreement between the experiment and the Maxwell modeling method described above. The first two plots illustrate the resistive load case in two different combinations of I_{P} and N. The remaining plots illustrate the constant voltage load case in two different combinations of I_{P} and N. Responses are almost identical in all configurations, indicating that the modeling accurately represents physical responses of the core under various settings of load type, I_{P}, and N. We can also infer that, by noticing that the peaks happen after the linear — unsaturated — regions, controlling the level of saturation of the core is necessary to extract the maximum magnetic energy from induction coupling.

Figure 10 presents time domain comparisons between the experiment and the Maxwell method where the waveforms of the load voltage in the resistive load case are depicted for three different saturation and load conditions.

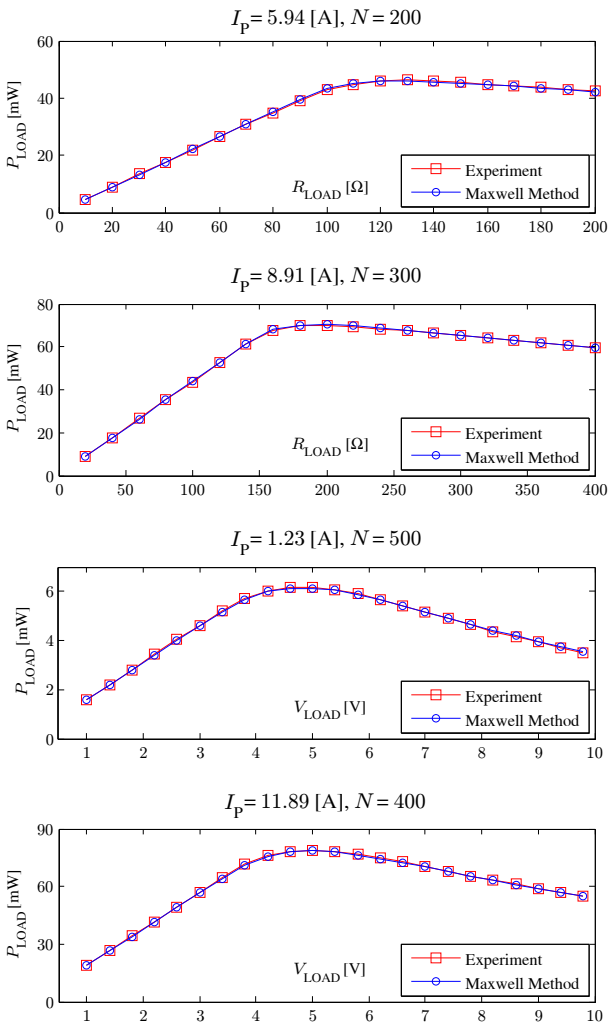

Fig. 9. Experimental verification of the Maxwell modeling method

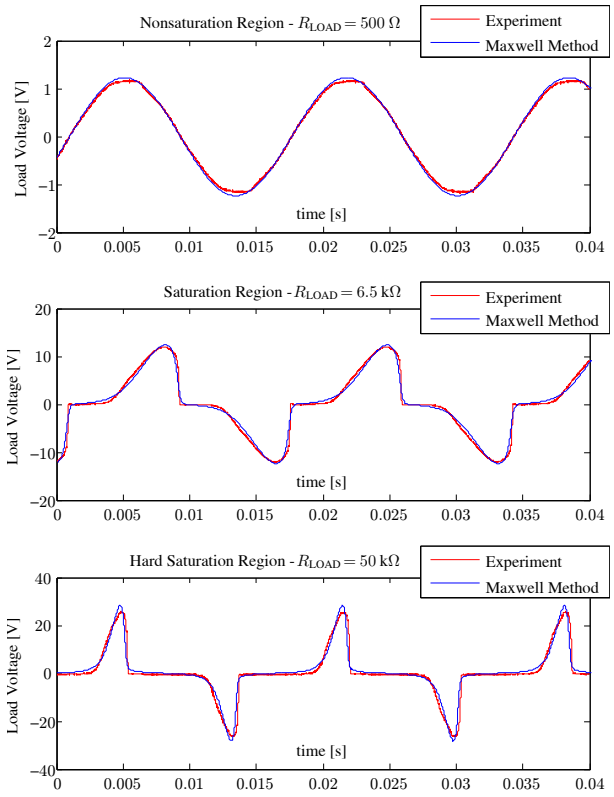

Fig. 10. Load voltage waveforms in experiments ($I_P = 1.23$ A, $N = 500$)

VII. Conclusion

This paper demonstrates that quick approximations can identify the transfer window for power transfer in a saturating current core. This analysis can be used for reasonably accurate decisions on core sizing and load targets for the magnetic energy harvester. A more accurate core model based on Maxwell's equations has been presented for precise numerical design simulation, where the B-H curve was modeled and nonideal losses were considered. Parameter estimation techniques for a physical core were demonstrated, and the numerical solver using Newton with GCR was presented. The solver has two layers: the first being the time range solver; and the second being a solver for steady-state and core loss resistance. Experimental results demonstrate the accuracy of the modeling approach for different loading conditions.

VIII. Acknowledgment

The authors thank the Kwanjeong Educational Foundation, the ONR Structural Acoustics Program and Debbie Nalchajian, and The Grainger Foundation.

References

[1] J. Moon, J. Donnal, J. Paris, S. Leeb, "VAMPIRE: A magnetically self-powered sensor node capable of wireless transmission," *Applied Power Electronics Conference and Exposition (APEC), 2013 Twenty-Eighth Annual IEEE*, Mar. 2013.

[2] J. Donnal, U. Orji, C. Schantz, J. Moon, S. Leeb, "VAMPIRE: Accessing a life-blood of information for maintenance and damage assessment," *Proc. American Society of Naval Engineers*, Feb. 2012.

[3] G. Herzer, "Amorphous and nanocrystalline soft magnets," *Proc. NATO Advanced Study Institute*, vol. 338, pp. 711-730, Jul. 1996.

[4] P. Dowell, "Effects of eddy currents in transformer windings," *Proc. IEE*, vol. 113, no. 8, pp. 1387-1394, Aug. 1966.

[5] S. Meninger, J. Mur-Miranda, R. Amirtharajah, A. Chandrakasan, and J. Lang, "Vibration-to-electric energy conversion," *IEEE Trans. Very Large Scale Integr. (VLSI) Syst.*, vol. 9, no. 1, pp. 64-76, Feb. 2001.

[6] G. Ottman, H. Hofmann, A. Bhatt, and G. Lesieutre, "Adaptive piezoelectric energy harvesting circuit for wireless remote power supply," *IEEE Trans. Power Electron.*, vol. 17, no. 5, pp. 669-676, Sep. 2002.

[7] I. Stark, "Thermal energy harevsting with thermo life," *IEEE Intl. Workshop on Wearable and Implantable Body Sensor Networks*, pp. 19-22, Apr. 2006.

[8] Y. Tan and S. Panda, "Energy harvesting from hybrid indoor ambient light and thermal energy sources for enhanced performance of wireless sensor nodes," *IEEE Trans. Ind. Electron.*, vol. 58, pp. 4424-4435, Sep. 2011.

[9] A. Fowler, S. Moheimani, and S. Behrens, "A 3-DoF MEMS ultrasonic energy harvester," *2012 IEEE Sensors*, pp. 1-4, Oct. 2012.

[10] J. Paradiso and T. Starner, "Energy scavenging for mobile and wireless electronics," *IEEE Pervasive Computing*, pp. 18-27, Jan. 2005.

[11] D. Brunelli, C. Moser, L. Thiele, and L. Benini, "Design of a solarharvesting circuit for batteryless embedded systems," *IEEE Trans. Circuits Syst. I, Reg. Papers*, vol. 56, no. 11, pp. 2519-2528, Nov. 2009.

[12] P. Mali, *Magnetic amplifiers - principles and applications*, New York, NY: John F. Rider Publisher, Inc., 1960.

[13] R. Watson and F. Lee, "Analysis, design, and experimental results of a 1-kW ZVS-FB-PWM converter employing magamp secondary-side control," *IEEE Trans. Ind. Electron.*, vol. 45, no. 5, pp. 806-814, Oct. 1998.

[14] E. da Silva, S. Abeyratne, and Y. Murai, "PWM series resonant DC-link converter with current clamping by the use of saturable core," *IEEE. Trans. Power Electron.*, vol. 14, no. 1, pp. 82-89, Jan. 1999.
[15] H. Gruening, K. Koyanagi, and M. Mukunoki, "Low reverse-recovery stress in high-power converters achieved by self-resetting saturable cores," *IEEE. Trnas. Ind. Appl.*, vol. 45, no. 1, pp. 232-238, Jan. 2009.
[16] S. Aldhaher, P. Luk, and J. Whidborne, "Tuning class E inverters applied in inductive links using saturable reactors," *IEEE Trans. Power Electron.*, vol. 29, no. 6, pp. 2969-2978, Jun. 2014.
[17] E. Snelling, *Soft ferrites - properties and applications*, 2nd Ed. Butterworth, UK: 1988.
[18] J. Li, T. Abdallah, and C. Sullivan, "Improved calculation of core loss with nonsinusoidal waveforms, *Proc. Industry Applications Society Conference*, vol. 4, pp. 2203-2210, Oct. 2001.
[19] K. Venkatachalam, C. Sullivan, T. Abdallah, and H. Tacca, "Accurate prediction of ferrite core loss with nonsinusoidal waveforms using only Steinmetz parameters," *Proc. IEEE Comput. Power Electron. Conf.*, pp. 36-41, Jun. 2002.
[20] Y. Han, G. Cheung, A. Li, C. Sullivan and D. Perreault, "Evaluation of magnetic materials for very high frequency power applications," *IEEE Trans. Power Electron.*, vol. 27, no. 1, pp. 425-435, Jan. 2012.
[21] J. Muhlethaler, J. Biela, J. Kolar, and A. Ecklebe, "Core losses under the DC bias condition based on Steinmetz parameters," *IEEE Trans. Power Electron.*, vol. 27, no. 2, pp. 953963, Feb. 2012.
[22] S. Eisenstat, H. Elman, and M. Schultz, "Variational iterative methods for nonsymmetric systems of linear equations," *SIAM J. Numer. Anal.*, vol. 20, no. 2, pp. 345-357, Apr. 1983.
[23] Y. Saad, *Iterative methods for sparse linear systems*, 2nd Ed. Philadelphia, PA: SIAM, 2003.